X-621-68-176
PREPRINT

FULL WAVE CALCULATIONS OF THERMOSPHERIC NEUTRAL AIR MOTIONS

H. Volland*

GODDARD SPACE FLIGHT CENTER
Greenbelt, Maryland

*On leave from the Astronomical Institutes of the University of Bonn, Germany, as a National Academy of Sciences-National Research Council Associate with the National Aeronautics and Space Administration.

FULL WAVE CALCULATIONS OF THERMOSPHERIC NEUTRAL AIR MOTIONS

H. Volland

ABSTRACT

Full wave calculations have been performed within the frequency range of gravity waves ($10^{-4} \leq \omega \leq 10^{-2}$ sec^{-2}) for a thermospheric model between 120 and 700 km altitude. In this altitude range gravity waves are coupled with heat conduction waves. Reflection, transmission, conversion and coupling from one wave type into the other one is described by the elements of the scattering matrix. The dependence of these elements on frequency and angle of incidence is discussed in full detail. The transmission coefficients of gravity waves calculated by full wave theory are compared with simple ray calculations and show that ray treatment is an excellent approximation for obliquely upward propagating gravity waves and that gravity waves predominate throughout the thermosphere. The thermosphere reacts like a selective filter with respect to upward propagating gravity waves with optimal transmission at $k_x \sim 2\omega$ (ω = angular frequency; k_x = horizontal wave number). Vertically downward propagating heat conduction waves are mainly converted into upward reflected gravity waves (at higher frequencies) or mainly coupled into downward propagating gravity waves (at lower frequencies).

FULL WAVE CALCULATIONS OF THERMOSPHERIC NEUTRAL AIR MOTIONS

1. Introduction

Satellite drag measurements of the neutral air density (Jacchia, 1959; Priester, 1959) have revealed for the first time that large scale diurnal variations of the density in thermospheric heights between 150 and at least 1200 km altitude exist, thermally driven by EUV heating from the sun (Harris and Priester, 1962). Hines (1960) put forward the hypothesis that free internal gravity waves of smaller periods generated within the lower atmosphere can propagate into the thermosphere. He suggested that travelling ionospheric disturbances observed within the F-region (see e.g., Heisler, 1967) are the response of the ionospheric plasma to these neutral air waves. Theoretical calculations especially those dealing with the ionospheric effect of the Russian H-bomb explosion of October 30, 1961 (Kohl, 1964; Row, 1967; Hines, 1967a) show surprising good agreement between the observed variations of the F-layer critical frequency at different stations and the theoretically expected dispersion effect of internal gravity waves depending on angle of incidence. Hines (1967a) could even explain the apparent period of the disturbance by a simple ray approach of the direction of energy propagation of gravity waves.

Recently, radar backscatter measurements (Thome, 1964) and HF-Doppler-effect measurements (Georges, 1967) as well as neutral air density observations

by pressure gauge measurements on board of Explorer 32 (Newton et al. 1968) have shown that wave like structure in the thermosphere reaches altitudes as high as 600 km. Hines (1967b) and Newton et al. (1968) using a ray treatment explained these waves again as free internal gravity waves propagating from the lower atmosphere up into the thermosphere. The most striking feature of these large altitude waves is the bending of the wave normals toward a horizontal direction with increasing altitude. In a ray treatment this bending is a dispersion effect due to energy dissipation of the waves [Hines (1967b); Newton et al. (1968)].

From the work of Harris and Priester (1962) and of Pitteway and Hines (1963) it can be suggested that heat conductivity is of predominating influence for the energy dissipation of neutral air waves. It can be shown numerically that the coefficient of viscosity can be neglected as compared with heat conductivity in thermospheric heights below 600 km and within the frequency range of gravity waves (Volland, 1968).

Under the influence of heat conduction, two different pairs of wave modes exist within the thermosphere: acoustic-gravity waves and heat conduction waves. They are coupled with each other at any height because their eigenvalues depend on the ratio

$$\frac{\kappa}{\bar{p}}$$

(κ = coefficient of heat conduction; $\bar{p}$ = mean pressure)

which increases with height, and therefore the thermosphere behaves like an inhomogeneous medium. Heat conduction waves are evanescent waves below about 200 km altitude. At higher altitudes, however, their attenuation rate is of the same order of magnitude as the attenuation rate of gravity waves. For these two reasons, the response of the thermosphere to the different wave modes including coupling and reflection processes must be determined by a full wave treatment, and a ray approximation has to be justified by these exact calculations.

Full wave calculations of neutral atmospheric waves in altitudes below 200 km have been performed by Midgley and Liehmon (1966). They calculated reflection coefficients of gravity waves and eliminated the evanescent heat conduction waves and viscosity waves by a special mathematical technique.

As pointed out above, this technique, which is fully justified at altitudes below 200 km, is not acceptable at greater heights because there heat conduction waves are no longer of an evanescent type.

This paper deals with a full wave treatment of neutral atmospheric waves at thermospheric heights taking into account heat conduction but neglecting viscosity, ion drag and Coriolis force. The negligence of the coefficient of viscosity is allowed at heights below 600 km and within the frequency range of gravity waves ($\omega \lesssim 10^{-2}$ sec^{-1}). The negligence of ion drag and Coriolis force is possible at frequencies

$$\omega > \begin{cases} \nu \\ 2\Omega \end{cases}$$

where Ω is the rotation period of the earth and ν is the collision frequency between neutrals and ions.

Our numerical calculations are extended to an altitude range of $120 \leqq Z \leqq 700$ km and a frequency range of $10^{-4} < \omega < 10^{-2}$ sec^{-1}. We shall compare these full wave calculations with simple ray approximation and shall mark the ranges of frequency, angle of incidence and wave type where a ray treatment is a sufficient approximation for neutral air wave propagation.

The mathematical background of full wave calculations is presented in Appendices A to E. For an understanding of the numerical results given in Section 4 only the contents of Sections 2 and 3, are necessary.

2. The Elements of the Scattering Matrix

As shown in Appendix A to C two pairs of characteristic waves exist within the neutral thermosphere which we collect by a column matrix [see Equation (C-1)].

$$\mathfrak{a} = \begin{pmatrix} a_G \\ a_H \\ b_G \\ b_H \end{pmatrix} \tag{1}$$

where a_G, b_G are ascending and descending gravity waves respectively, and a_H, b_H are ascending and descending heat conduction waves, respectively.

Our model atmosphere consists of three regions (see Figure 1). The regions below Z_I (region I) and above Z_{II} (region III) are considered as homogeneous (G = const) and isothermal ($\bar{T}$ = const) atmospheres extended infinitely into the half spaces. The region between Z_I and Z_{II} (region II) approximates part of the real atmosphere. Its parameters approach the parameters of regions I and III at the boundaries Z_I and Z_{II}, respectively.

Coupling between the four characteristic waves then only occurs within region II, while in regions I and III the waves are uncoupled with each other. The connection between the four waves at the lower boundary Z_I with the four waves at the upper boundary Z_{II} of region II is given by Equation (D-6):

$$a^{II}(Z_{II}) = P_I^{II}\, a^I(Z_I) \tag{2}$$

We are mainly interested in reflection and transmission coefficients of the different waves. These coefficients are the elements of the scattering matrix well known in electromagnetic wave propagation (see e.g., Volland, 1962). The scattering matrix connects the waves going into region II with the waves coming out of region II:

$$\begin{aligned} b^I &= R^I a^I + T^{II} b^{II} \\ a^{II} &= T^I a^I + R^{II} b^{II} \end{aligned} \tag{3}$$

where we introduced column matrices of ascending and descending waves:

$$\mathbf{a} = \begin{pmatrix} a_G \\ \\ a_H \end{pmatrix}; \quad \mathbf{b} = \begin{pmatrix} b_G \\ \\ b_H \end{pmatrix},$$

$\mathbf{R}^{I}$ and $\mathbf{R}^{II}$ are (2×2) — reflection matrices, and $\mathbf{T}^{I}$ and $\mathbf{T}^{II}$ are (2×2) — transmission matrices. We collect these last four matrices into a (4×4) scattering matrix:

$$\mathbf{S}_I^{II} = \begin{pmatrix} \mathbf{R}^{I} & \mathbf{T}^{II} \\ \\ \mathbf{T}^{I} & \mathbf{R}^{II} \end{pmatrix}. \tag{4}$$

A simple algebraic transformation leads to relations between the submatrices of $\mathbf{S}_I^{II}$ and the submatrices of $\mathbf{P}_I^{II}$ in Equation (2)

$$\begin{aligned} \mathbf{R}^{I} &= -\mathbf{P}_4^{-1}\,\mathbf{P}_3 \\ \mathbf{R}^{II} &= \mathbf{P}_2\,\mathbf{P}_4^{-1} \\ \mathbf{T}^{I} &= \mathbf{P}_1 - \mathbf{P}_2\,\mathbf{P}_4^{-1}\,\mathbf{P}_3 \\ \mathbf{T}^{II} &= \mathbf{P}_4^{-1} \end{aligned} \tag{5}$$

where

$$\mathbf{P}_I^{II} = \begin{pmatrix} \mathbf{P}_1 & \mathbf{P}_2 \\ \\ \mathbf{P}_3 & \mathbf{P}_4 \end{pmatrix}.$$

The elements of $\mathbf{S}_I^{II}$ completely describe the behavior of region II with respect to plane waves. It is e.g.,

$$\mathbf{R}^I = \begin{pmatrix} {}_G R_G^I & {}_G R_H^I \\ {}_H R_G^I & {}_H R_H^I \end{pmatrix} \tag{6}$$

where the elements

$${}_G R_G^I = \frac{b_G^I}{a_G^I}\,; \quad {}_H R_H = \frac{b_H^I}{a_H^I}$$

are related to the reflection of gravity waves (G) or heat conduction waves (H) coming from below.

$${}_H R_G^I = \frac{b_H^I}{a_G^I}\,; \quad {}_G R_H^I = \frac{b_G^I}{a_H^I}$$

are conversion coefficients transferring part of the incoming wave energy of one wave type into reflected wave energy of the other wave type. Equivalent relations hold for the other three submatrices $\mathbf{R}^{II}$, $\mathbf{T}^I$ and $\mathbf{T}^{II}$.

Figure 1 shows the four elements of the first column of matrix $\mathbf{S}_I^{II}$ [Equation (4)] which give the ratios between reflected and transmitted waves, respectively, and an incoming gravity wave from below.

Twelve equivalent elements for the three other incoming waves exist but are only outlined in Figure 1.

The elements a_i and b_i have the dimension $\sqrt{\text{Energy/Area}}$.

Therefore $R \cdot R^*$ and $T \cdot T^*$ (a star indicates conjugate complex values) are measures of the reflected and transmitted wave energy per area. But note the difficulties arising from an incomplete definition of energy in Appendix E.

3. Atmospheric Model and Numerical Techniques

For the model atmosphere in region II we chose the Harris-Priester model 5 at 12^{00} local time (CIRA, 1965). The lower boundary of region II is Z_I = 120 km. Below Z_I an isothermal atmosphere with the temperature at the height Z_I is added as region I. The upper boundary Z_{II} serves as parameter running from Z_I to 600 km. Region III then is an isothermal atmosphere with the temperature in the height Z_{II}. For some calculations (results shown in Figure 7) a height Z_{II} = 700 km has been fixed and Z_I was a parameter.

Note that in order to make regions I and III homogeneous with respect to characteristic waves the coefficient of heat conductivity κ in these regions must decrease exponentially with altitude like the pressure [see Equation (A-4)]. As will be seen later this is not a serious limitation for the acceptance of that model because below 100 km heat conduction waves are purely evanescent waves (their wave amplitude is attenuated by a factor larger than $\frac{1}{e}$ = 0.37 after

propagating 1 km in the vertical direction), and gravity wave propagation is only slightly influenced by heat conductivity. The region above 600 km otherwise has no influence on the reflection characteristics of gravity waves.

Region II is approximated by a number of homogeneous isothermal slabs of thickness ΔZ_ν = 1 km. Again in each slab it is $\frac{\kappa}{p}$ = const. Repeated calculations with changing $\Delta Z_\nu \geq 100$ m did not show significant differences in the results and indicate that our model with slab thickness ΔZ_ν = 1 km is a sufficient approximation of a realistic atmosphere.

If one starts calculations at heights below 200 km where the attenuation rate of heat condition waves increases rapidly, one is confronted with a practical difficulty in numerical techniques. The elements of $\mathbf{P}_I^{II}$ in Equation (1) can become very large in magnitude, and the elements of $\mathbf{T}^I$ in Equation (5) are differences of two large values. If these differences are smaller than the accuracy of the computer, the numerical results of the elements of $\mathbf{T}^I$ become meaningless. In order to determine $\mathbf{T}^I$ under these circumstances one has to repeat the calculations starting from the top of region II and calculating downward. Then the error of $\mathbf{T}^I$ is small enough while now $\mathbf{T}^{II}$ becomes meaningless below a certain altitude.

4. Numerical Results

In this section we shall give numerical results for the elements of the scattering matrix determined from Equations (D-6) and (5).

Figure 2 gives the magnitude of the four elements ${}_{G}R_{G}^{I}$, ${}_{H}R_{G}^{I}$, ${}_{G}T_{G}^{I}$ and ${}_{H}T_{G}^{I}$ which describe reflection, conversion, transmission and coupling into heat conduction waves of incoming gravity waves from below. The frequency used is $\omega = 10^{-3}$ sec^{-1} (equivalent to a period of $t = \frac{2\pi}{\omega} = 105$ min), the horizontal wave number used is $k_x = 10^{-2}$ km^{-1} (equivalent to a horizontal wavelength of $\lambda_x = \frac{2\pi}{k_x} = 628$ km).

The transmission coefficient ${}_{G}T_{G}^{I}$ decreases in this altitude range by a factor of 170. The mean pressure decreases in the same height interval by a factor of 420. Therefore the amplitude ratio of the gravity wave between 120 and 600 km is [see Equation (A-3)]

$$\sqrt{\frac{C_I \bar{P}_I}{C_{II} \bar{P}_{II}}} \left| {}_{G}T_{G}^{I} \right| = 0.25$$

large enough to be detectable.

The reflection coefficient ${}_{G}R_{G}^{I}$ remains constant at altitudes above 250 km. Its value of 8×10^{-2} is equivalent to a reflected energy of 6.4×10^{-3} of the incoming energy. The conversion coefficient ${}_{H}R_{G}^{I}$ which converts part of the incoming gravity wave energy into reflected heat conduction wave energy, has the value 5×10^{-3} and remains constant above an altitude of 200 km. The constancy of the reflection factors indicates that the region above 250 km has no influence on the reflection characteristics of the atmosphere below 120 km.

The coupling coefficient ${}_{H}T_{G}^{I}$ which is responsible for the transfer of energy from the gravity mode into heat conduction mode never exceeds 3% of the magnitude of the transmission coefficient ${}_{G}T_{G}^{I}$. Therefore not more than 1‰ of the gravity wave energy is coupled into heat conduction wave energy.

In Figure 3 the transmission coefficient ${}_{G}T_{G}^{I} \hat{=} T_{W}$ has been compared with the transmission coefficient T_{R} derived from a simple ray approximation [Equation (D-7)]. Here magnitude (Figure 3a) and phase (Figure 3b) are plotted versus height using the same frequency as in Figure 2 and two different values of k_{x}. As seen in Figure 3 ray calculation (dashed lines) is an excellent approximation in this range of frequency and horizontal number in heights above 200 km. The discrepancy between full wave and ray calculations at $k_{x} = 2.15 \times 10^{-3}$ km arises mainly in the height region below 200 km where the temperature gradient of the atmospheric model is largest.

Note that the thickness of the whole thermosphere in terms of the vertical wavelength of gravity waves is only of the order of one wavelength.

In order to test the range of validity of the ray approximation the ratio between the magnitudes of both transmission coefficients $\left|\frac{T_{W}}{T_{R}}\right|$ and the difference of their phase values in 600 km height have been plotted versus horizontal wave number k_{x} in Figure 4a again for $\omega = 10^{-3}$ sec^{-1}. Small horizontal wave numbers mean steep incidence of the waves.

In the range $k_x \lesssim 10^{-3}$ km^{-1} the ray approximation breaks down. This is the range of horizontal wavelengths where gravity waves are totally reflected within the lower atmosphere (see Figure 4b). In the range $k_x > 10^{-3}$ km^{-3} maximum discrepancy occurs in the phase at $k_x = 2.15 \times 10^{-3}$ km^{-1}. But from Figure 3b we observe that this discrepancy already is generated within the height region $Z < 200$ km. Therefore a ray approximation is valid at this value of k_x in heights $Z \gtrsim 200$ km.

In Figure 4b the magnitudes of the four elements ${}_GR_G^I$, ${}_HR_G^I$, ${}_GT_G^I$ and ${}_HT_G^I$ discussed in Figure 2 have been calculated for a region II range from 120 to 600 km and are plotted versus horizontal wave number k_x. In the range $k_x < 2 \times 10^{-3}$ km^{-1} the reflection coefficient $|{}_GR_G^I|$ becomes larger than 1 indicating the difficulty in the definition of energy (see Appendix E). Therefore the elements are normalized according to Equation (E-8) in this region (dashed lines) and only give upper limits.

There is a maximum in the magnitude of the transmission coefficient ${}_GT_G^I$ near $k_x = 2 \times 10^{-3}$ km^{-1} showing that the atmosphere behaves like a selective transformer depending on frequency and horizontal wave number.

Otherwise the pressure amplitude of gravity waves at frequency $\omega = 10^{-3}$ sec^{-1} and horizontal wave numbers $k_x > 1.5 \times 10^{-2}$ km^{-1} has dropped to values $< 10^{-1}$ after travelling through region II from 120 to 600 km height and becomes difficult to detect.

In the whole range of k_x the coupling coefficient ${}_HT_G^I$ is negligibly small compared with ${}_GT_G^I$. The conversion coefficient ${}_HR_G^I$ is also small. Gravity waves therefore predominate throughout the entire thermosphere, and heat conduction waves are unimportant for the transport of wave energy within the thermosphere.

Figures 5 and 6 calculated for the two angular frequencies $\omega = 10^{-4}$ sec^{-1} and $\omega = 10^{-2}$ sec^{-1} give similar results to Figure 4. In Figure 5 we observe essentially the same behavior as in Figure 4 only shifted toward one smaller magnitude of k_x. Now ray approximation is valid for horizontal wavenumbers $k_x > 10^{-4}$ km^{-1}, and the maximum discrepancy in phase at $k_x \sim 2 \times 10^{-4}$ km^{-1} in Figure 5a is again generated below Z = 200 km. Detectable wave amplitudes of gravity waves are expected to have wave numbers between $2 < 10^{-4} \lesssim k_x < 2 \times 10^{-3}$ km^{-1}.

Figure 6 has been calculated for an angular frequency of $\omega = 10^{-2}$ sec^{-1} and a height region between 200 and 600 km because this frequency is strongly reflected below 200 km. Now there is no maximum in the transmission coefficient ${}_GT_G^I$ in Figure 6b because at this frequency the wave with index G behaves like a gravity wave at $k_x > 10^{-2}$ km^{-1} [real part of eigenvalue α_G negative for upgoing waves (see Appendix B)] and behaves like acoustic wave at $k_x < 10^{-2}$ km^{-1} (α_G positive for upgoing wave). In the gravity wave range a ray approximation is valid. Within the acoustic range the transmission coefficient ${}_GT_G^I$ is nearly

constant. Coupling into heat conduction waves again is negligible within the whole range of k_x at this frequency.

Figure 7 (full lines) finally show reflection ($_HR_H^{II}$), transmission ($_HT_H^{II}$), conversion ($_GR_H^{II}$) and coupling ($_GT_H^{II}$) into gravity waves of downgoing heat conduction waves at vertical incidence ($k_x = 0$) and for two different frequencies ($\omega = 10^{-3}$ sec^{-1} in Figure 7a; $\omega = 10^{-4}$ sec^{-1} in Figure 7b). The model region II starts now in 700 km, and the elements are calculated as functions of Z_I and are plotted versus altitude. Here we note that some elements of the scattering matrix exceed the value one. This peculiar behavior has already been observed for ascending gravity waves at steep incidence and shows the incompleteness of the energy definition (see Appendix E). No attempt has been made however to normalize the numerical values in Figure 7 with the help of a condition equivalent to Equation (E-8). Therefore only the relative relations between the different elements can be discussed. We see from Figure 7a that in altitudes below 500 km most of the energy of heat conduction waves of frequency $\omega = 10^{-3}$ sec^{-1} has been converted into gravity waves the larger part reflected, the rest transmitted into the lower regions.

Figure 7b shows the same data but for the smaller frequency $\omega = 10^{-4}$ sec^{-1}. There below 600 km most of the energy is already converted and coupled into gravity waves. But now coupling predominates. Ray approximation, of course, becomes senseless under these conditions because of the strong coupling effect.

Therefore the statements in the paper of Volland (1967), which are based on ray approximation of vertically downward propagating heat conduction waves, must be modified.

For comparison the transmission coefficient ${}_{G}T_{G}^{II}$ of downward propagating gravity waves is plotted as dashed lines in Figure 7. In Figure 7b this coefficient below 500 km is smaller by two orders of magnitudes than the coupling coefficient ${}_{G}T_{H}^{II}$. Therefore we expect from this result that the vertical downward transport of energy is mainly due to this coupling from heat conduction waves into gravity waves.

Unfortunately it is not possible at the present state to derive from Figure 7 a quantitative value for the amount of energy transfer through the thermosphere. We only can find from Equation (A-3) an upper limit for the ratio between the amplitude of a gravity wave at 120 km and the amplitude of a heat conduction wave at 700 km taking $|{}_{G}T_{H}^{II}| \leq 1$ as

$$\sqrt{\frac{C_{II}\ \bar{\rho}_{II}}{C_{I}\ \bar{\rho}_{I}}}\ |{}_{G}T_{H}^{II}| \leq 1.5 \times 10^{-2}$$

which shows that these waves are no longer detectable in 120 km altitude.

5. Concluding Remarks

Numerical full wave calculations have been performed within the frequency range of gravity waves ($10^{-4} \leqq \omega \leqq 10^{-2}$ sec^{-1}) in thermospheric heights between 120 and 700 km. In these heights coupling occurs between gravity waves and

heat conduction waves. These calculations have been compared with those for simple ray approximation. It has been shown that

1. Ray treatment is an excellent approximation for obliquely upward propagating gravity waves at horizontal wave numbers $k_x \gtrsim \omega$.

2. The rate of coupling from gravity wave energy into heat conduction energy is negligibly small for upward propagating gravity waves. Gravity waves therefore predominate the upward transport of wave energy within the thermosphere.

3. The thermosphere reacts like a selective filter with respect to gravity wave. The range of optimal transmission is near $k_x \sim 2\omega$.

4. At $\omega = 10^{-3}$ sec^{-1} the energy of vertically downward propagating heat conduction waves is mainly converted into ascending gravity waves. At $\omega = 10^{-4}$ sec^{-1} however the larger part of the energy of vertically downward propagating heat conduction waves is coupled into downward propagating gravity waves.

These calculations suffer from one uncertainty. This is the incomplete definition of the energy flux for the single waves resulting in reflection and transmission coefficients with magnitudes larger than 1, which happens at steep and vertical incidence. No way has been found to overcome this difficulty.

APPENDIX A

The Basic Equations

Since we deal with gravity waves of periods $10^{-4} < \omega < 10^{-2}$ sec^{-1} at heights below 600 km we can neglect the coefficient of viscosity, ion drag and Coriolis force. We moreover consider only the simplest wave form, namely plane, nonducted, harmonic waves of angular frequency ω propagating obliquely into a quiet horizontally stratified, isothermal atmosphere. The parameters of the atmosphere are only functions of altitude Z. The propagation plane shall be the (X - Z) -plane of a Cartesian coordinate system. A strict perturbation method then leads to a system of first order differential equations (Volland, 1968)

$$\frac{d\mathbf{e}}{dZ} = jk\,\mathbf{K}\mathbf{e} \qquad (A\text{-}1)$$

where

$$\mathbf{e}(Z) = \begin{pmatrix} e_1 \\ e_2 \\ e_3 \\ e_4 \end{pmatrix}$$

$$e_1 = \sqrt{\frac{\bar{p}}{C}}\,\Delta w$$

$$e_2 = \sqrt{\frac{C}{\bar{p}}}\,\Delta p$$

$$e_3 = \sqrt{\frac{\bar{\rho}C}{\bar{T}}}\,\Delta T$$

$$e_4 = \frac{\kappa}{\sqrt{\bar{\rho}C}}\,\frac{d\Delta T}{dZ}$$

$$\Delta u = \sqrt{\frac{C}{\bar{p}}}\,\frac{S}{\gamma}\,e_2$$

$$\Delta\rho = \frac{\bar{\rho}}{\sqrt{\bar{\rho}C}}\,(e_2 - e_3)$$

Δu, Δw, Δp, ΔT, $\Delta\rho$ = wave amplitudes of { horizontal velocity; vertical velocity; pressure; temperature; density }

C, $\bar{p}(Z)$, $\bar{T}$, $\bar{\rho}(Z)$ = time independent values of { acoustic phase velocity; pressure; temperature; density }

κ coefficient of heat conductivity

$\gamma = \frac{c_p}{c_v}$ ratio of specific heats at constant pressure and constant volumn

$S = \frac{k_x}{k}$ normalized horizontal wavenumber

$$K(Z) = \begin{pmatrix} -jA & -\left(1 - \frac{S^2}{\gamma}\right) & 1 & 0 \\ -\gamma & jA & -2jA & 0 \\ 0 & 0 & jA & \frac{-2jG}{d} \\ -2jA & -1 & d\left(1 + \frac{S^2}{2jG}\right) & -jA \end{pmatrix}$$

k_x = horizontal wave number in X-direction considered as real and constant

$k = \frac{\omega}{C}$ wave number of acoustic waves

ω = angular frequency considered as real and constant

$C = \sqrt{\gamma \frac{R}{M} \bar{T}}$ acoustic phase velocity

R = gas constant

M = molecular weight

$A = \frac{\omega_a}{\omega}$

$G = \frac{\omega_h}{\omega}$

$d = \frac{\gamma}{\gamma - 1}$

$$\omega_a = \frac{\gamma g}{2C}$$

$$\omega_h = \frac{\gamma g}{2V}$$

$V = \frac{\kappa g}{c_p \bar{\rho}}$ heat conduction velocity

g = gravitational acceleration

The wave amplitudes of horizontal velocity Δu and of density $\Delta\rho$ are linearly related with e_2 and e_3 and do not appear explicitly in system Equation (A-1).

The e_k are normalized in such a manner that their dimension is $\sqrt{\text{Energy/Area}}$. Thus the amplitude increase of the wave within an adiabatic isothermal atmosphere like

$$e^{-\frac{Z}{2H}} \tag{A-2}$$

($H = \frac{R\bar{T}}{Mg}$ is the scale height)

is already compensated, and the squares of the normalized wave amplitudes $e_K e_K^*$ are related to the energy flux of the wave.

The ratio of the pressure amplitudes of the perturbation relative to the mean atmospheric pressure in two different heights Z_I and Z_{II} is

$$\frac{\bar{p}_{II}}{\bar{p}_I} \frac{\Delta p_I}{\Delta p_{II}} = \frac{\sqrt{\bar{p}_I C_I}}{\sqrt{\bar{p}_{II} C_{II}}} \frac{e_2^{II}}{e_2^I} \tag{A-3}$$

The same expressions hold for the other physical parameter.

The height dependence of **K** in Equation (A-1) within an isothermal atmosphere comes only through the parameter G (Z) because κ = const, but

$$p = p_0 e^{-Z/H} \tag{A-4}$$

Since we shall approximate the real atmosphere by a number of homogeneous isothermal slabs we have to choose within one slab G = const. which implies

$$p \propto \kappa = \kappa_0 e^{-Z/H} \tag{A-5}$$

APPENDIX B

Characteristic Waves and Eigenvalues

If the coefficient matrix **K** in Equation (A-1) is constant we can define ascending and descending characteristic waves by

$$\left.\begin{matrix} a_i \\ b_i \end{matrix}\right\} \sim e^{\mp j k q_i Z} \tag{B-1}$$

We call q_i the eigenvalue of the i-th characteristic wave. Within the isothermal atmosphere it is

$$q_i = \sqrt{\frac{\gamma}{2} - A^2 - S^2 - jG \pm \sqrt{\left(\frac{\gamma}{2} - jG\right)^2 + 2jG(1 + B^2 S^2)}} \tag{B-2}$$

with

$$B = \sqrt{\frac{(\gamma - 1)}{\gamma}}\, A = \frac{\omega_b}{\omega}$$

(ω_b = Brunt-Vaisälä-frequency)

The plus sign inside the square root in Equation (B-2) is associated with the pair of acoustic-gravity waves [an ascending one (a_1) and a descending one (b_1)]. The minus sign is associated with heat conduction waves (a_2, b_2).*

---

*For reasons of clarity we shall refer in Sections 2 to 4 to $a_1 \rightarrow a_G$ $\quad b_1 \rightarrow b_G$
$a_2 \rightarrow a_H$ $\quad b_2 \rightarrow b_H$

The terms "ascending" and "descending" are related to the direction of energy propagation. Wave energy is dissipated by heat conduction, governed by the parameter G in Equation (B-2), which leads to complex eigenvalues

$$q_1 = \alpha_i - j\,\beta_i \qquad \text{(B-3)}$$

From Equation (B-1) it follows then that wave energy of an upgoing wave [minus sign in Equation (B-1)] is dissipated if

$$\beta_i > 0 \qquad \text{(B-3)}$$

regardless of whether α_i is positive or negative. α_1 is negative for the gravity mode. This is a distinctive mark for that wave type. Within a nondissipative atmosphere $G \to \infty$. Then acoustic-gravity waves become inattenuated ($\beta_1 = 0$) while heat conduction waves become evanescent waves ($\beta_2 \to \infty$).

APPENDIX C

The Transformation Matrix **Q**

The transformation from the physical parameters e_k in Equation (A-1) into the parameters of the single characteristic waves a_i is defined by

$$\mathbf{e} = \mathbf{Q}\,\mathbf{a} \tag{C-1}$$

where

$$\mathbf{a} = \begin{pmatrix} a_1 \\ a_2 \\ b_1 \\ b_2 \end{pmatrix}$$

is the column matrix of the characteristic waves and **Q** can be found from the system of linear equations

$$(\mathbf{K} + q_i \mathbf{E})\,\mathbf{Q}_i = 0 \tag{C-2}$$

where $\mathbf{Q}_i$ is the i-th column matrix of **Q** and **E** is the unit matrix. We obtain as elements of **Q**

$$Q_{ki} = L_{ki} \frac{F_i}{\sqrt{2 q_i \delta_i}} \tag{C-3}$$

with

$$L_{1i} = q_i - jA\left\{1 - \frac{2S^2}{\gamma}\right\}$$

$$L_{2i} = \gamma - 2A^2 - 2jAq_i$$

$$L_{3i} = \gamma - S^2 - A^2 - q_i^2$$

$$L_{4i} = \frac{dL_{3i}}{2jG}(q_i + jA)$$

$$\delta_i = \begin{cases} 1 & i = 1,2 \\ \text{for} & \\ -1 & i = 3,4 \end{cases}$$

$$q_3 = -q_1$$

$$q_4 = -q_2.$$

F_i are arbitrary normalization factors which can be taken e.g., as

$$F_i = 1.$$

But note their significance in the WKB-approximation [see Equation (D-10)].

Furthermore we need the reciprocal $\mathbf{Q}^{-1}$ of the matrix $\mathbf{Q}$ which has the elements:

$$(Q^{-1})_{i1} = -E_i L_{3i+1} L_{2i+2} \Lambda \delta_i$$

$$(Q^{-1})_{i2} = E_i L_{3i+1} L_{1i+2} \Lambda \delta_i$$

$$(Q^{-1})_{i3} = E_i (q_i - jA) \delta_i$$

$$(Q^{-1})_{i4} = E_i \frac{2jG}{d} \delta_i$$

with

$$E_i = \frac{1}{(L_{3i} - L_{3i+1}) F_i \sqrt{2 q_i \delta_i}}$$

$$\Lambda = \frac{1}{\gamma - \frac{4 S^2 A^2}{\gamma}}$$

APPENDIX D

Exact Solution of Equation (A-1) and Ray Approximation

Within a homogeneous slab Equation (A-1) can be transformed with help of Equation (C-1) into

$$\frac{d\mathbf{a}}{dZ} = j\,k\,\mathbf{N}\,\mathbf{a} \tag{D-1}$$

with

$$\mathbf{N} = \mathbf{Q}^{-1}\,\mathbf{K}\,\mathbf{Q} = \begin{pmatrix} -q_1 & 0 & 0 & 0 \\ 0 & -q_2 & 0 & 0 \\ 0 & 0 & q_1 & 0 \\ 0 & 0 & 0 & q_2 \end{pmatrix} \tag{D-2}$$

Within the ν-th slab of thickness $\Delta Z_\nu = Z_\nu - Z_{\nu-1}$ Equation (D-1) has the solution

$$\mathbf{a}_\nu(Z_\nu) = e^{jk_\nu \mathbf{N}_\nu \Delta Z_\nu}\,\mathbf{a}_\nu(Z_{\nu-1}) \tag{D-3}$$

which is equivalent to Equation (B-1).

At the boundary between two slabs total pressure, vertical velocity, temperature and heat flux of the wave amplitude must be continuous (see Appendix E). This leads to (see Figure D-1)

$$\Gamma_{\nu+1}\,e_{\nu+1}\Big|_{Z_\nu+0} = \Gamma_\nu\,e_\nu\Big|_{Z_\nu-0} \tag{D-4}$$

with

$$\Gamma_\nu(Z) = \frac{1}{\sqrt{C_\nu \bar{p}_\nu}} \begin{pmatrix} C_\nu & 0 & 0 & 0 \\ 0 & \bar{p}(Z) & 0 & 0 \\ 0 & 0 & \bar{T}_\nu & 0 \\ 0 & 0 & 0 & \bar{p}(Z) C_\nu \end{pmatrix} \qquad \text{(D-5)}$$

The general solution of Equation (A-1) for wave propagation within an atmosphere composed of n homogeneous slabs is then:

$$\mathbf{a}_n(Z_n) = \mathbf{P}_0^n \, \mathbf{a}_0(Z_0) \qquad \text{(D-6)}$$

with

$$\mathbf{P}_0^n = \prod_{\nu=1}^{n} e^{jk_\nu N_\nu \Delta z_\nu} \, \mathbf{Q}_\nu^{-1} \, \Gamma_\nu^{-1}(Z_{\nu-1}) \, \Gamma_{\nu-1}(Z_{\nu-1}) \, \mathbf{Q}_{\nu-1}$$

If the parameters of two adjacent slabs only slightly differ from each other then

$$\mathbf{Q}_\nu^{-1} \, \Gamma_\nu^{-1}(Z_{\nu-1}) \, \Gamma_{\nu-1}(Z_{\nu-1}) \, \mathbf{Q}_{\nu-1} \sim \mathbf{E} \,,$$

and the approximate ray solution of Equation (D-6) is

$$\mathbf{a}_n(Z_n) \sim e^{j \int_{Z_0}^{Z_n} k \mathbf{N} \, d\xi} \, \mathbf{a}_0(Z_0) \qquad \text{(D-7)}$$

where now $k(Z)$ $q_i(Z)$ are considered as continuous functions of altitude. The physical parameters of the i-th characteristic wave according to Equation (C-1) are

$$e_k(Z) = \mathbf{Q}_{ki}(Z)\, a_i(Z) \tag{D-8}$$

The approximation Equation (D-7) becomes optimal if one normalizes the elements of $\mathbf{Q}$ in such a manner that

$$\mathbf{Q}^{-1}\frac{d\mathbf{Q}}{dZ} = \begin{pmatrix} 0 & \cdot & \cdot & \cdot \\ \cdot & 0 & \cdot & \cdot \\ \cdot & \cdot & 0 & \cdot \\ \cdot & \cdot & \cdot & 0 \end{pmatrix} \tag{D-9}$$

contains only zeros within the diagonal.

This condition leads to a unique determination of the factor F_i in Equation (C-3):

$$F_i = \exp\left\{-\int_{z_0}^{z} \frac{L_{3i}}{4H}\left\{\frac{\left(\frac{\gamma}{2} - jG\right)}{D_i^2} - \frac{jA}{q_i D_i}\right\} d\xi\right\} \tag{D-10}$$

with

$$D_i = L_{3i} - \frac{\gamma}{2} - jG\,.$$

Equation (D-8) with the normalization condition Equation (D-9) is known as WKB-approximation.

APPENDIX E

Energy Flux

The equation of conservation of energy neglecting viscosity can be written as (see e.g., Volland, 1967)

$$\frac{\partial}{\partial t}(E + U + \chi) + \operatorname{div} \vec{S} = Q \qquad \text{(E-1)}$$

$E = \frac{\rho}{2} v^2$ (kinetic energy)

$U = c_v \rho T$ (internal energy)

$\chi = -\rho g (Z - Z_o)$ (potential energy)

$Q =$ (external energy source)

$$S_m = (E + U + \chi + p)\, v_m - \kappa \frac{\partial T}{\partial x_m} \qquad \text{(E-2)}$$

(component of energy flux vector $\vec{S}$ in m-direction)

Z_o is the height of an arbitrary reference level of potential energy. Its significance is not quite clear, and we set $\chi = 0$. The kinetic energy E is of third order and can be neglected.

If there is no external energy source ($Q = 0$) as we assumed throughout this paper then the vertical component S_z must be continuous at any level. This implies pressure p, temperature T, vertical velocity v_z and vertical heat flux $-\kappa \frac{\partial T}{\partial Z}$ to be continuous at any boundary.

The effective energy flux of the i-th characteristic wave is given by the time average of S_m:

$$\left.\begin{matrix}\overline{S_x} \\ \overline{S_z}\end{matrix}\right\}_i = \frac{1}{2}\,\text{Real}\left\{\frac{\gamma}{\gamma-1}\,\Delta p\begin{pmatrix}\Delta u^* \\ \Delta w^*\end{pmatrix}\right\}_i = \frac{1}{4}\frac{\gamma}{(\gamma-1)}\begin{Bmatrix}\frac{2S}{\gamma}\,e_2 e_2^* \\ (e_2 e_1^* + e_2^* e_1)\end{Bmatrix} \qquad \text{(E-3)}$$

(The star indicates complex conjugate values.) The vertical time averaged heat flux is canceled out because

$$\kappa\frac{d\,\Delta T}{dZ} = \sqrt{\bar{p}\,C}\,e_4$$

in Equation (A-1) and

$$\overline{e}_k = 0\,.$$

Unfortunately the direction θ_e of energy flux derived from Equation (E-3)

$$\text{tg}\theta_e = \left(\frac{\overline{S_x}}{S_z}\right)_i = \frac{S\left[(\gamma - 2A^2 - 2A\beta_i)^2 + 4A^2\alpha_i^2\right]}{\alpha_i\,(\gamma^2 - 4A^2S^2)} \qquad \text{(E-4)}$$

does not coincide with ray direction θ_r derived by

$$\text{tg}\theta_r = -\frac{\partial\alpha_i}{\partial S} = \text{Real}\left\{\frac{S}{q_i}\left[1 - \frac{j\,GB^2}{q_i^2 + A^2 - \frac{\gamma}{2} + S^2 + j\,G}\right]\right\} \qquad \text{(E-5)}$$

as long as $\kappa \neq 0$. Only for $G \to \infty$ ($\kappa = 0$) do both directions become equal for gravity waves:

$$tg\theta_e = tg\theta_r = \frac{S}{\alpha_1}(1 - B^2) \qquad (\kappa = 0) \qquad \text{(E-6)}$$

We observe the same discrepancy as in electromagnetic wave propagation where the direction of the Poynting vector and the ray direction differ from each other within a dissipative plasma. (See e.g., Hines, 1951.) Equation (E-3) therefore is no definite measure of energy flux. Whether or not the neglect of potential energy is the reason for this discrepancy is not clear to us.

In view of these difficulties we do not try to use Equation (E-3) for the determination of energy flux but simply consider the values $a_i\, a_i^*$ calculated from solution Equation (D-6) as measure of energy flux of the different characteristic waves.

If the amplitudes a_i are clearly related to wave energy flux then the magnitudes of the elements of the scattering matrix [see Equation (4)] should be always smaller than 1. In the numerical results of Section 4 we shall find, especially at steep incidence, magnitudes of some reflection and transmission coefficients larger than 1. This indicates that our definition of energy flux is incomplete resulting from the difficulties outlined above.

From general energy considerations however we can give an upper limit for the magnitude of the elements of the scattering matrix. Imagine that only a gravity wave penetrates into region II from below (see Figure 1). Then Equation (3) leads to

$$\begin{pmatrix} b_G^I \\ b_H^I \\ a_G^{II} \\ a_H^{II} \end{pmatrix} = \begin{pmatrix} {}_GR_G^I \\ {}_HR_G^I \\ {}_GT_G^I \\ {}_HT_G^I \end{pmatrix} a_G^I \qquad \text{(E-7)}$$

Since all waves are decoupled from each other in regions I and III and since energy leaving region II can not exceed energy penetrating region II then

$$({}_GR_G^I)^2 + ({}_HR_G^I)^2 + ({}_GT_G^I)^2 + ({}_HT_G^I)^2 \leq 1 \qquad \text{(E-8)}$$

where the equal sign in Equation (E-8) applies only in the case of a nondissipative atmosphere ($\kappa = 0$).

From Equation (E-8) and equivalent equations holding for the other 12 elements we can normalize the R and T. This has been done partly in Figures 4 and 5.

LITERATURE

CIRA, COSPAR International Reference Atmosphere, 1965, North-Holland Publishing Company, Amsterdam, 1965.

Georges, T. M., HF-Doppler Studies of travelling ionospheric disturbances, AGARD XIII Symposium on Phase and Frequency Instability in Electromagnetic Wave Propagation, Ankara, Turkey, Oct., 1967.

Harris, I. and W. Priester, Time dependent structure of the upper atmosphere, Journ. Atmospheric Sci., 19, 286-301, 1962.

Heisler, L. H., Travelling ionospheric disturbances, Space Research VII, p. 55-66, North-Holland Publishing Company, Amsterdam, 1967.

Hines, C. O., Wave packets, the Poynting vector and energy flow, Part I to IV, Journ. Geophys. Res. 56, 63-72, 197-206, 207-220, 535-544, 1951.

Hines, C. O., Internal gravity waves in ionospheric heights, Can. Journ. Phys. 38, 1441-1481, 1960.

Hines, C. O., On the nature of travelling ionospheric disturbances launched by low altitude nuclear explosions, Journ. Geophys. Res. 72, 1877-1882, 1967a.

Hines, C. O., Some consequences of dissipative effects in the propagation of atmospheric gravity waves in the F-region, IAGA/URSI Symposium on

Upper Atmospheric Winds, Waves, and Ionospheric Drifts, St. Gallen, Switzerland, Oct., 1967b.

Jacchia, L. G., Solar effects on the acceleration of artificial satellites, Smithson. Astrophys. Obs. Spec. Rep. No. 29, 1959.

Kohl, H., Acoustic gravity waves caused by the nuclear explosion on October 30th, 1961, Electron density distribution in Ionosphere and Exosphere; Thrane (ed.), p. 160-169, North-Holland Publishing Company, Amsterdam, 1964.

Midgley, J. E. and H. B. Liehmon, Gravity waves in a realistic atmosphere, Journ. Geophys. Res. 71, 3727-3748, 1966.

Newton, G. P., Pelz, D. T. and H. Volland, Direct, in situ measurements of wave propagation in the neutral thermosphere, submitted to Journ. Geophys. Res., 1968.

Pitteway, M. L. V. and C. O. Hines, The viscous damping of atmospheric gravity waves, Can. Journ. Phys. 71, 1935-1948, 1963.

Priester, W., Sonnenaktivität und Abbremsung der Erdsatelliten, Naturwissenschaften, 46, 197-198, 1959.

Row, R. V., Localized low altitude sources and acoustic gravity wave perturbations of the ionosphere, AGARD XIII Symposium on Phase and Frequency Instability in Electromagnetic Wave Propagation, Ankara, Turkey, Oct. 1967.

Thome, G. D., Incoherent scatter observations of travelling ionospheric disturbances, Journ. Geophys. Res. 69, 4047-4049, 1964.

Volland, H., The propagation of plane electromagnetic waves in a horizontally stratified ionosphere, Journ. Atm. Terr. Phys., 24, 853-857, 1962.

Volland, H., Heat conduction waves in the upper atmosphere, Journ. Geophys. Res. 72, 2831-2841, 1967.

Volland, H., The upper atmosphere as a multiple refractive medium for neutral air motions, submitted to Journ. Atm. Terr. Phys., 1968.

FIGURE CAPTIONS

Figure 1. Elements of the scattering matrix. Reflection coefficients (R) and transmission coefficients (T) of upward (a) and downward (b) propagating gravity waves (G) and heat conduction waves (H) within the thermosphere.

Figure 2. Magnitude of coefficients of reflection (${}_GR_G^I$), transmission (${}_GT_G^I$), conversion (${}_HR_G^I$) and coupling (${}_HT_G^I$) into heat conduction waves of upward propagating gravity waves versus Z_{II}.

Figure 3. Magnitude (Figure 3a) and phase (Figure 3b) of transmission coefficients of upward propagating gravity waves calculated by full wave theory (full lines) and by ray approximation (dashed lines).

Figure 4a. Ratio between transmission coefficients of upward propagating gravity waves calculated by full wave theory (W) and ray theory (R) versus horizontal wave number k_x. Range of thermospheric model: 120 to 600 km; angular frequency: $\omega = 10^{-3}$ sec^{-1}.

Figure 4b. Magnitude of coefficients of reflection, transmission, conversion and coupling into heat conduction waves of upward propagating gravity waves versus horizontal wave number k_x. Range of thermospheric model: 120 to 600 km. Angular frequency: $\omega = 10^{-3}$ sec^{-1}. Dashed lines give upper limits (for details see text).

Figure 5. Same as text of Figure 4, but angular frequency: $\omega = 10^{-4}$ sec^{-1}.

Figure 6. Same as text of Figure 4, but angular frequency: $\omega = 10^{-2}$ sec^{-1}; range of thermospheric model 200 - 600 km.

Figure 7. Full lines: Magnitude of coefficients of reflection, transmission, conversion and coupling into gravity waves of vertically downward propagating heat conduction waves versus Z_I.

Dashed lines: Magnitude of transmission coefficients of vertically downward propagating gravity waves.

Figure 7a. $\omega = 10^{-3}$ sec^{-1}.

Figure 7b. $\omega = 10^{-4}$ sec^{-1}.

Figure D-1. The homogeneous slab-model.

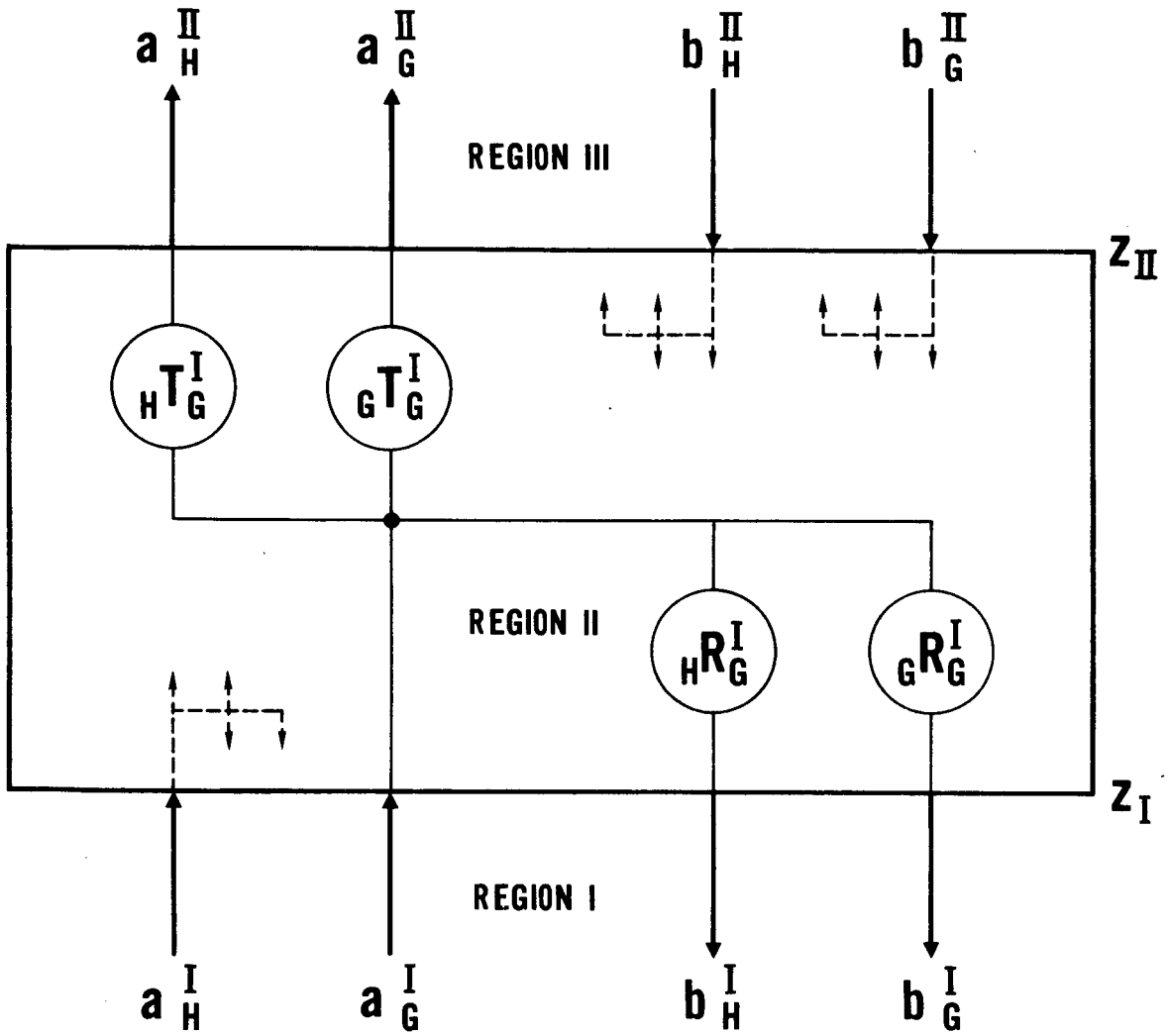

Figure 1. Elements of the scattering matrix. Reflection coefficients (R) and transmission coefficients (T) of upward (a) and downward (b) propagating gravity waves (G) and heat conduction waves (H) within the thermosphere.

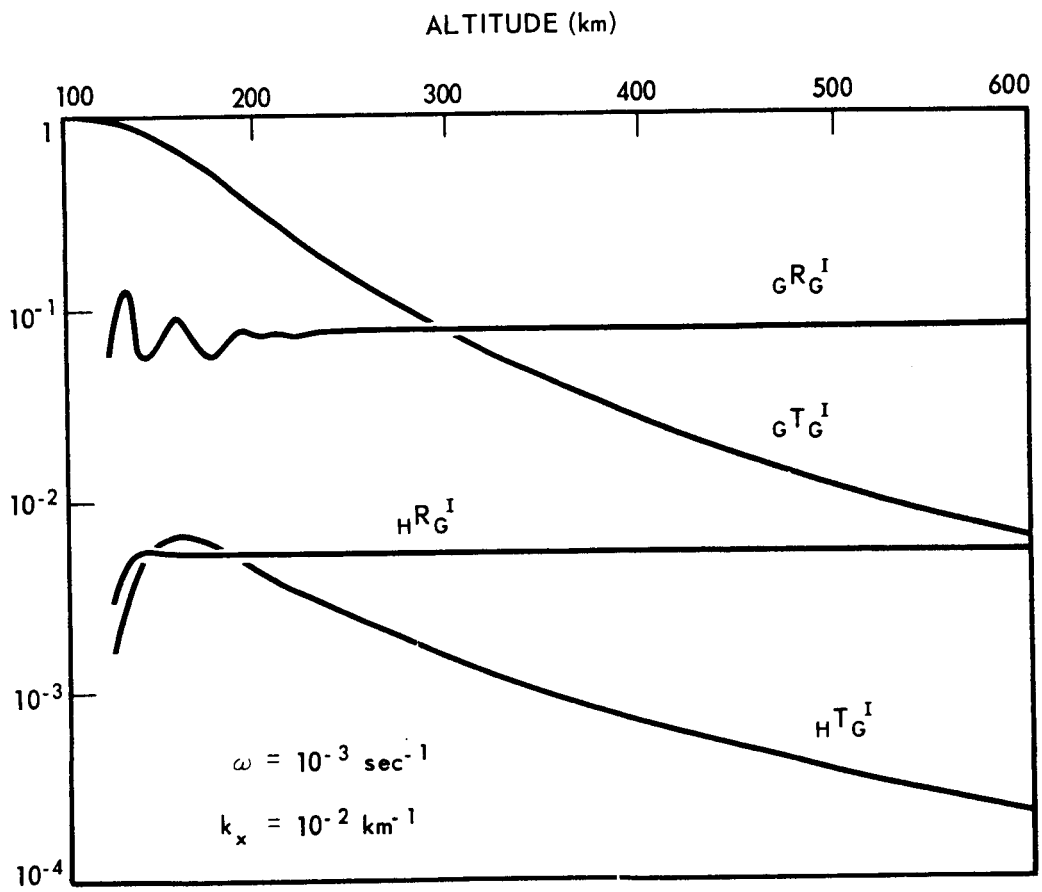

Figure 2. Magnitude of coefficients of reflection ($_GR_G^I$), transmission ($_GT_G^I$), conversion ($_HR_G^I$) and coupling ($_HT_G^I$) into heat conduction waves of upward propagating gravity waves versus Z_{II}.

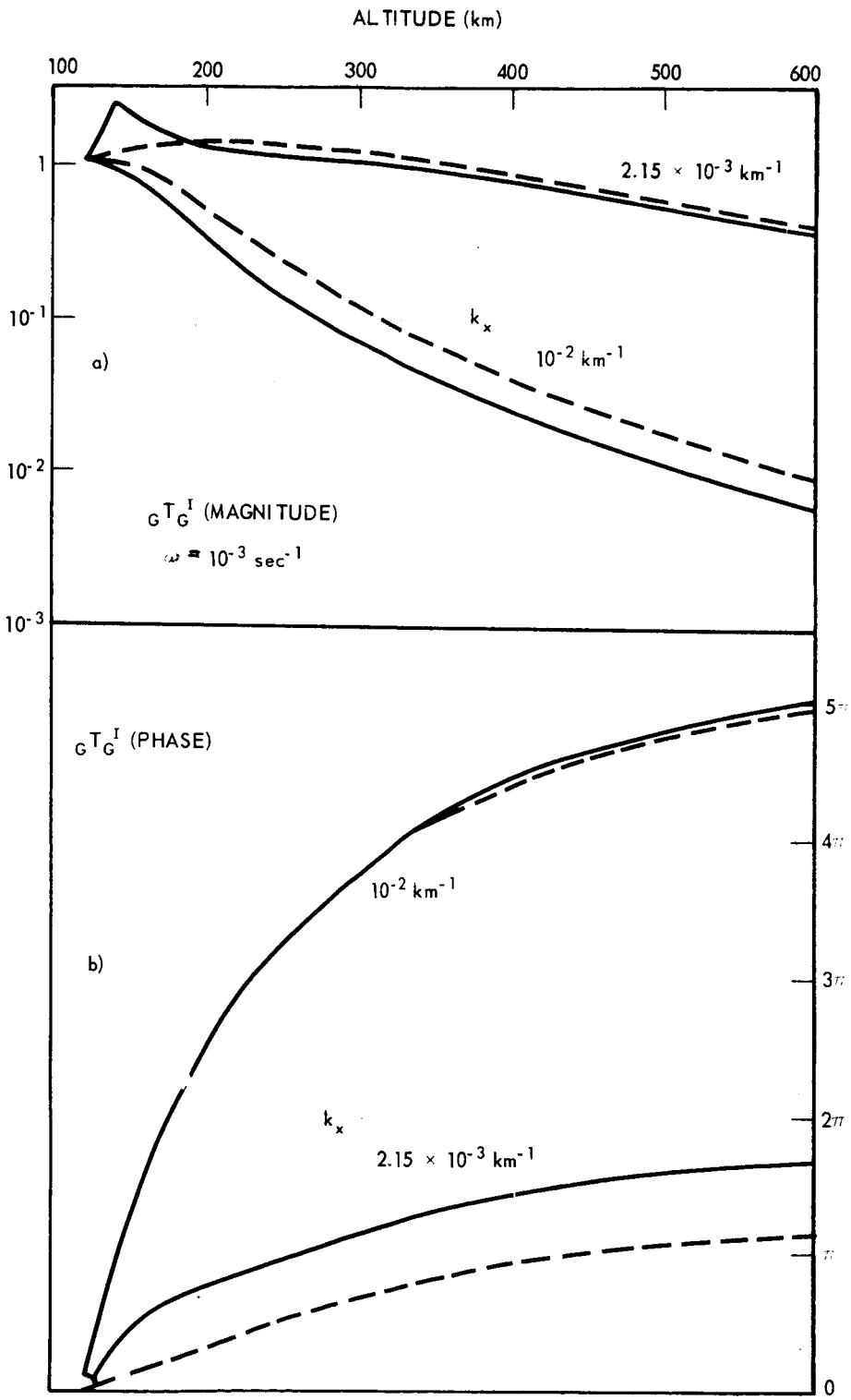

Figure 3. Magnitude (Figure 3a) and phase (Figure 3b) of transmission coefficients of upward propagating gravity waves calculated by full wave theory (full lines) and by ray approximation (dashed lines).

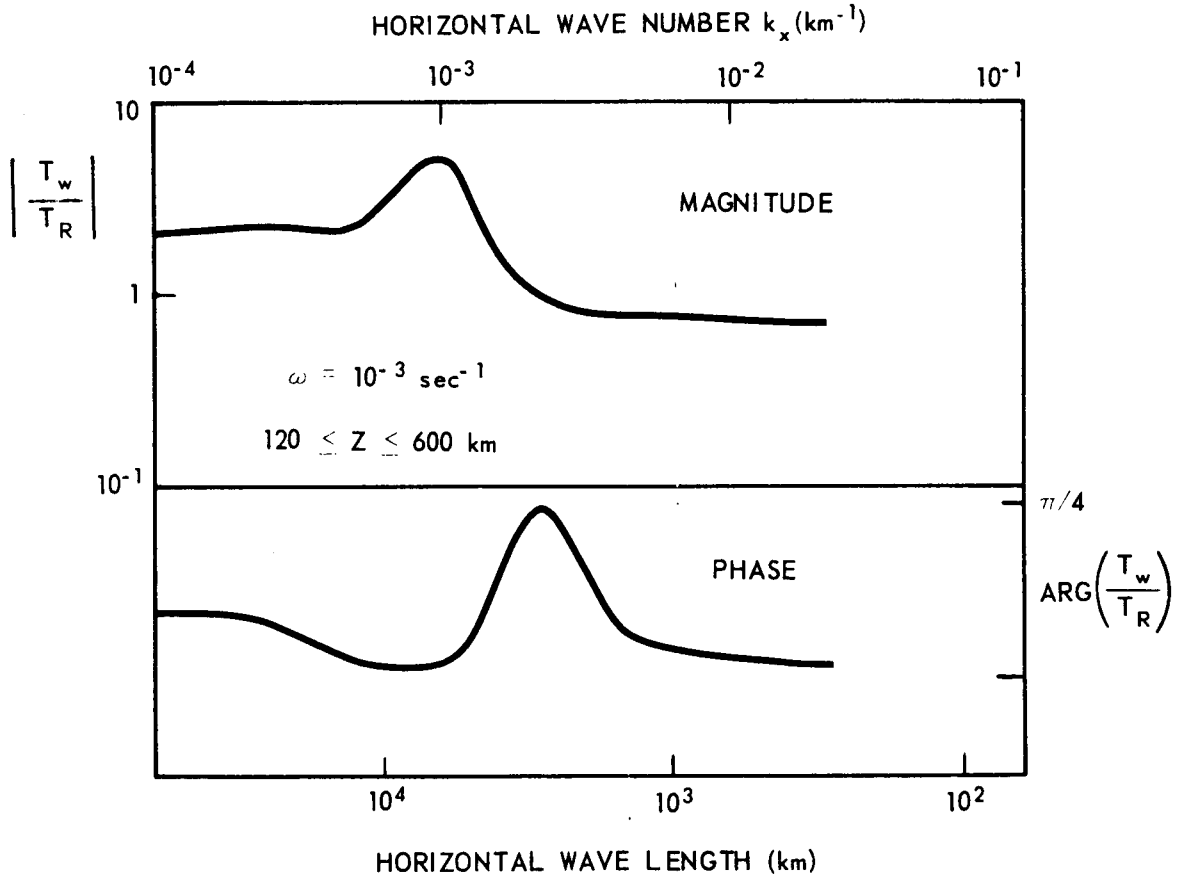

Figure 4a. Ratio between transmission coefficients of upward propagating gravity waves calculated by full wave theory (W) and ray theory (R) versus horizontal wave number k_x. Range of thermospheric model: 120 to 600 km; angular frequency: $\omega = 10^{-3}$ sec^{-1}.

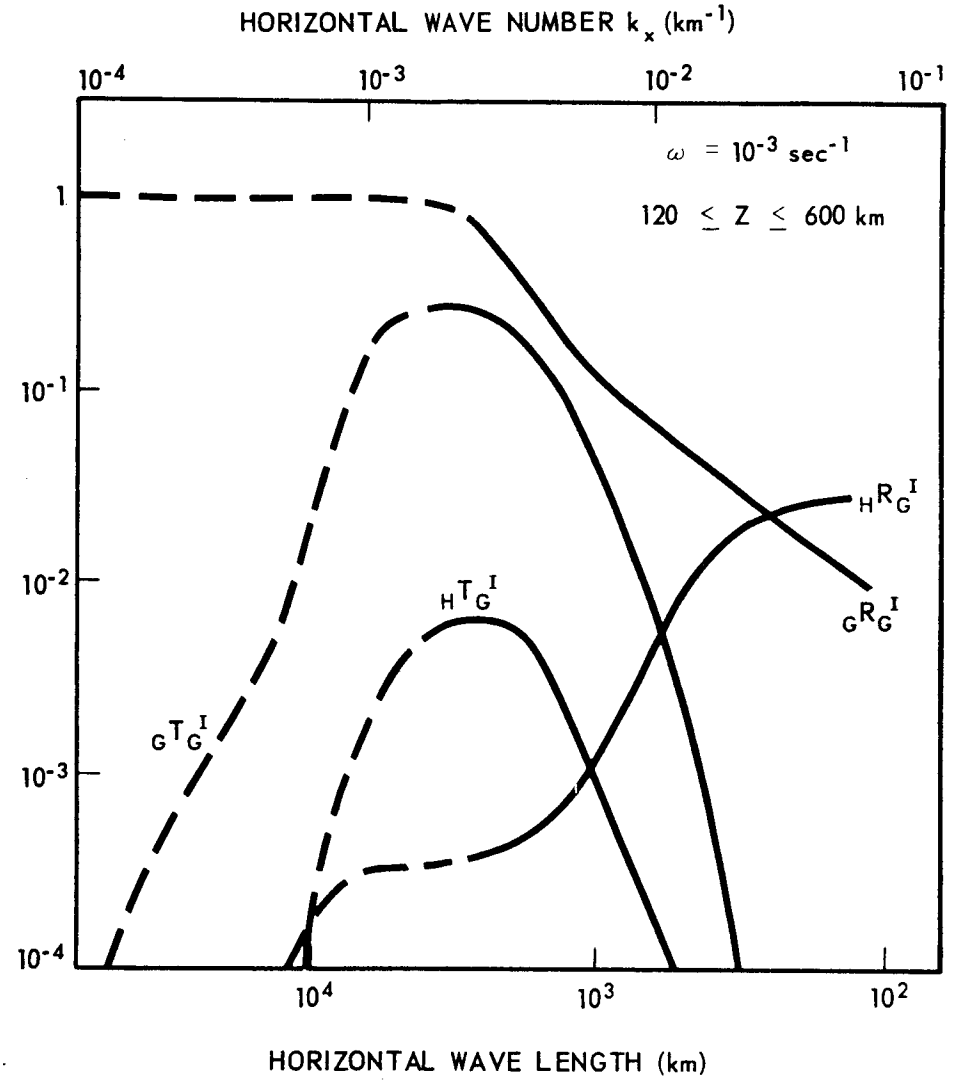

Figure 4b. Magnitude of coefficients of reflection, transmission, conversion and coupling into heat conduction waves of upward propagating gravity waves versus horizontal wave number k_x. Range of thermospheric model: 120 to 600 km. Angular frequency: $\omega = 10^{-3}$ sec^{-1}. Dashed lines give upper limits (for details see text).

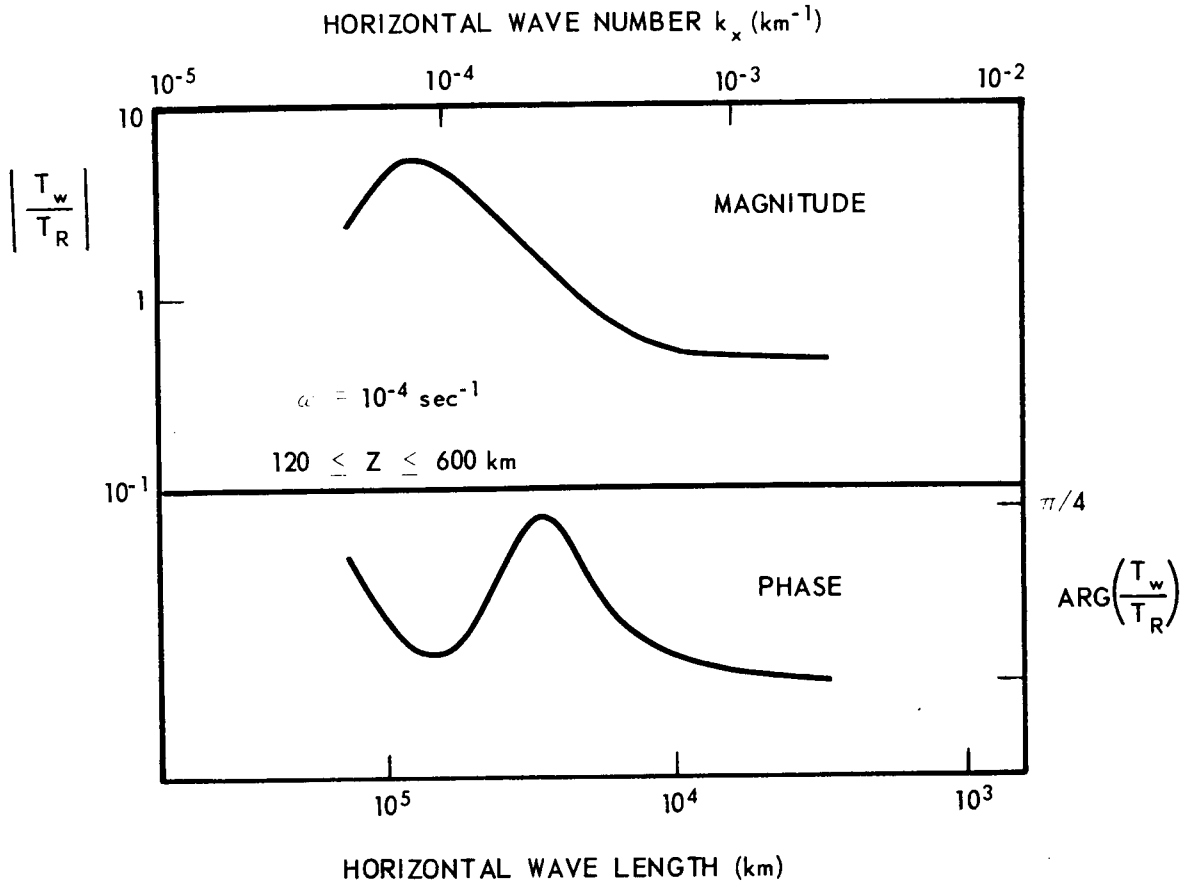

Figure 5a. Same as text of Figure 4, but angular frequency: $\omega = 10^{-4}$ sec^{-1}.

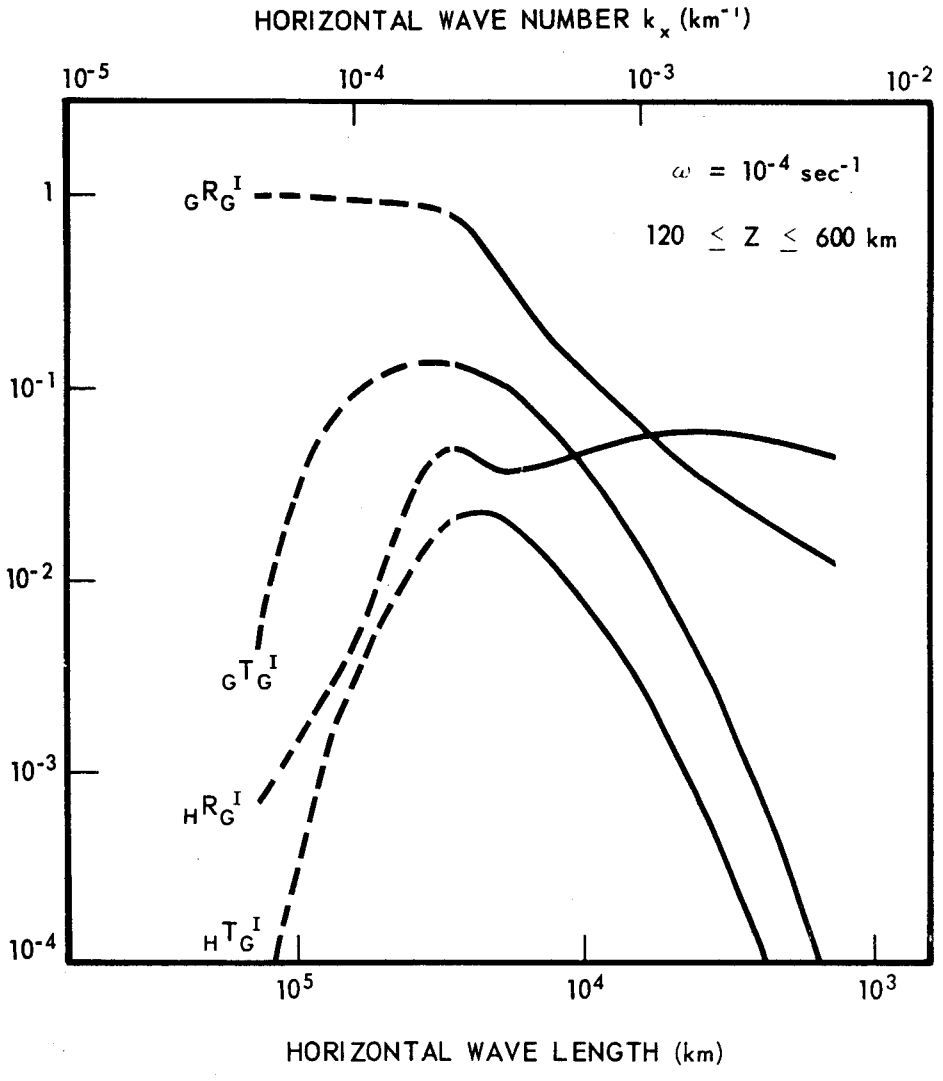

Figure 5b. Same as text of Figure 4, but angular frequency: $\omega = 10^{-4}$ sec^{-1}.

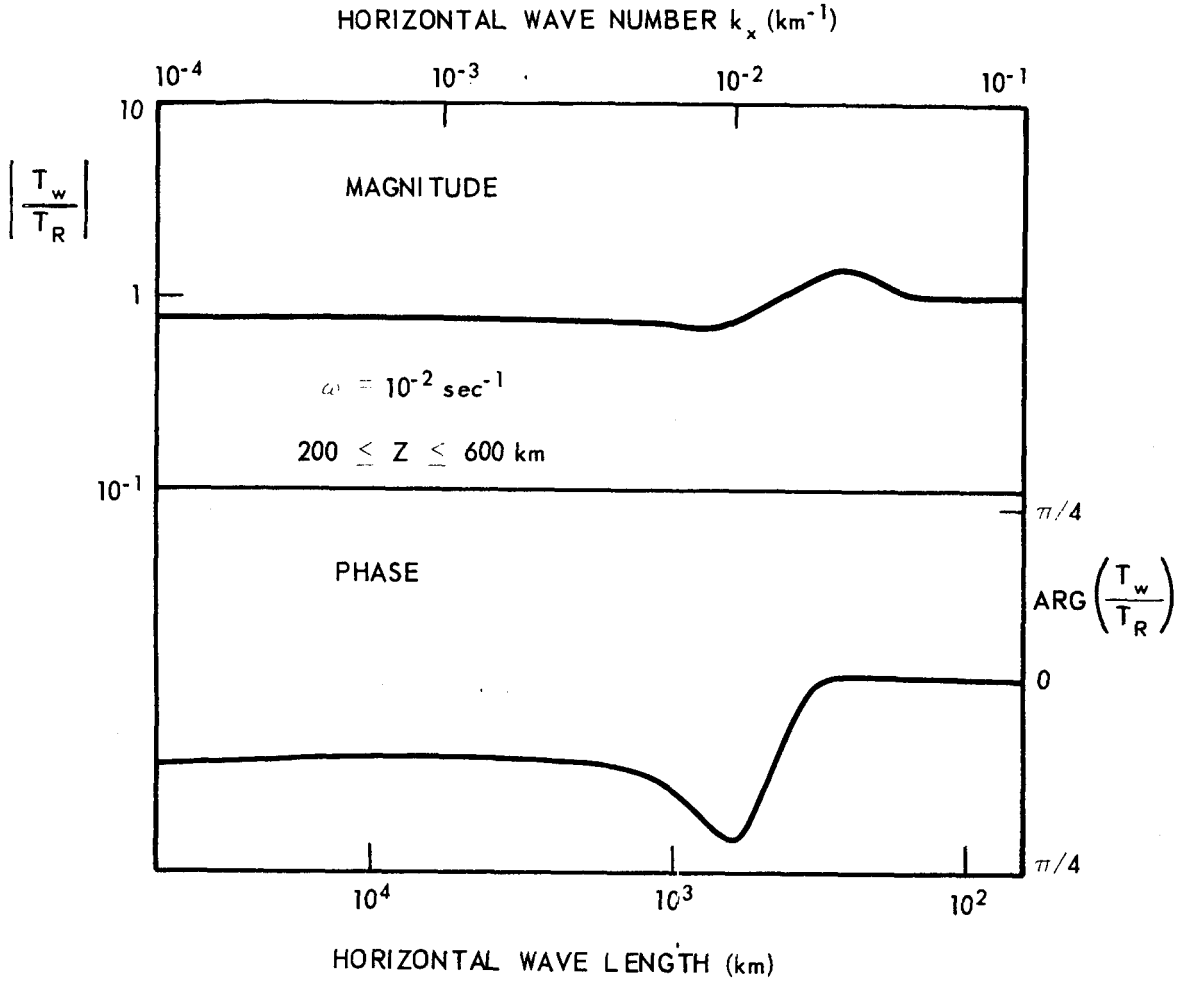

Figure 6a. Same as text of Figure 4, but angular frequency: $\omega = 10^{-2}$ sec^{-1}; range of thermospheric model 200 – 600 km.

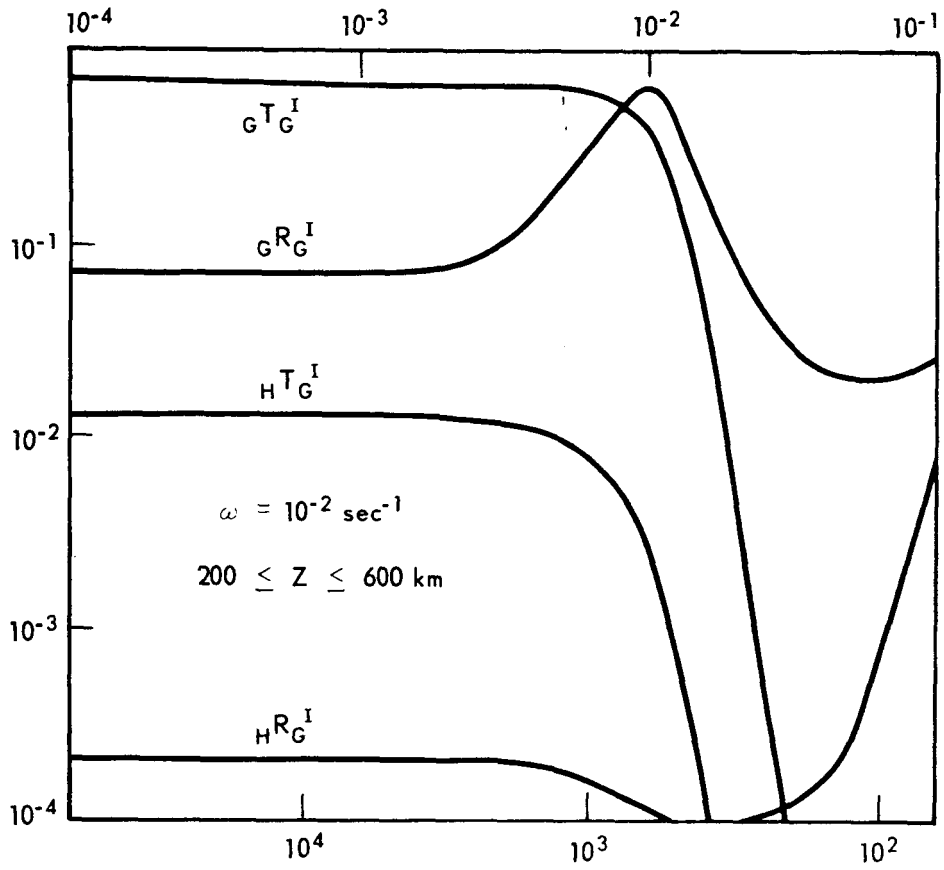

Figure 6b. Same as text of Figure 4, but angular frequency: $\omega = 10^{-2}$ sec^{-1}; range of thermospheric model 200 – 600 km.

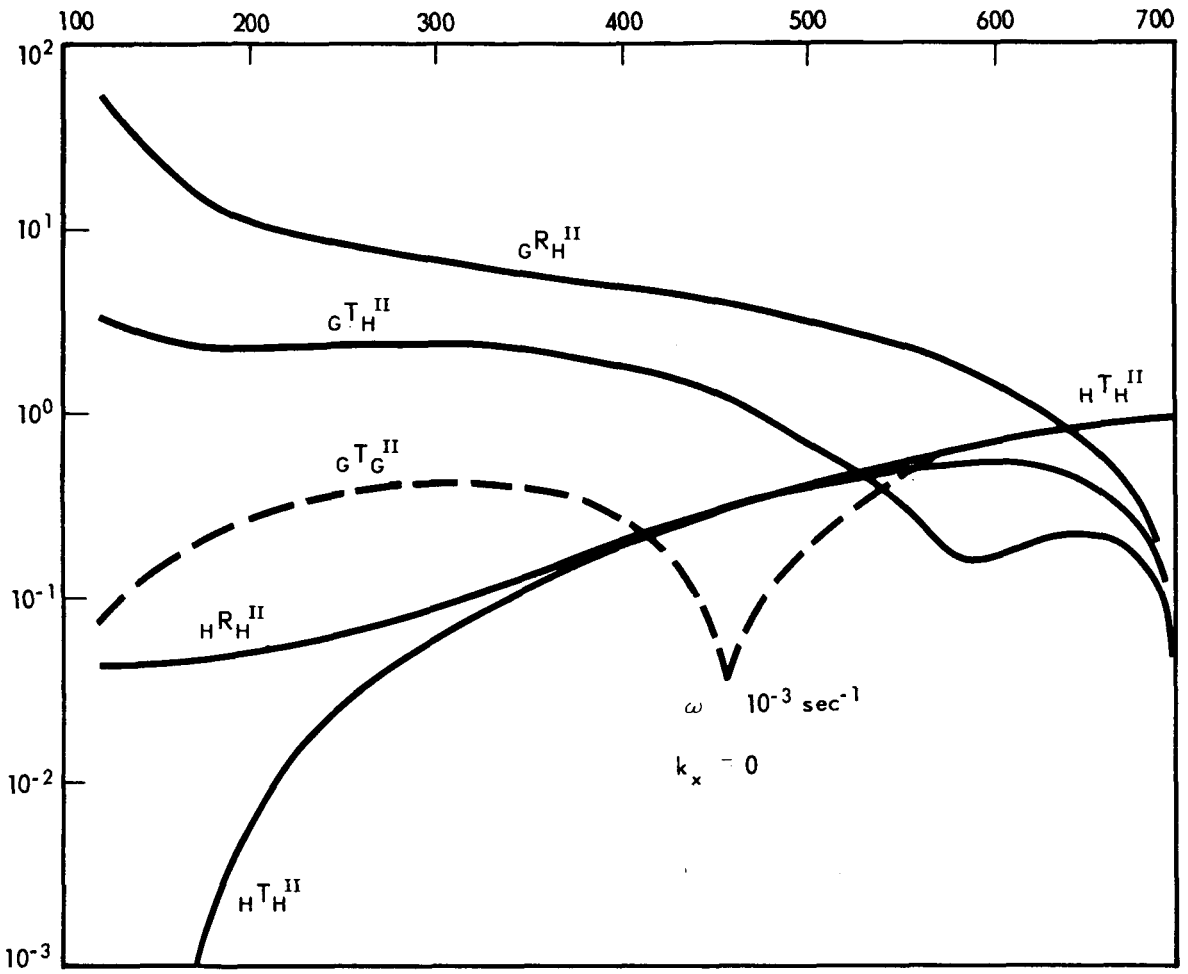

Figure 7a. Full lines: Magnitude of coefficients of reflection, transmission, conversion and coupling into gravity waves of vertically downward propagating heat conduction waves versus Z_I.

Dashed lines: Magnitude of transmission coefficients of vertically downward propagating gravity waves. Angular frequency: $\omega = 10^{-3}$ sec^{-1}.

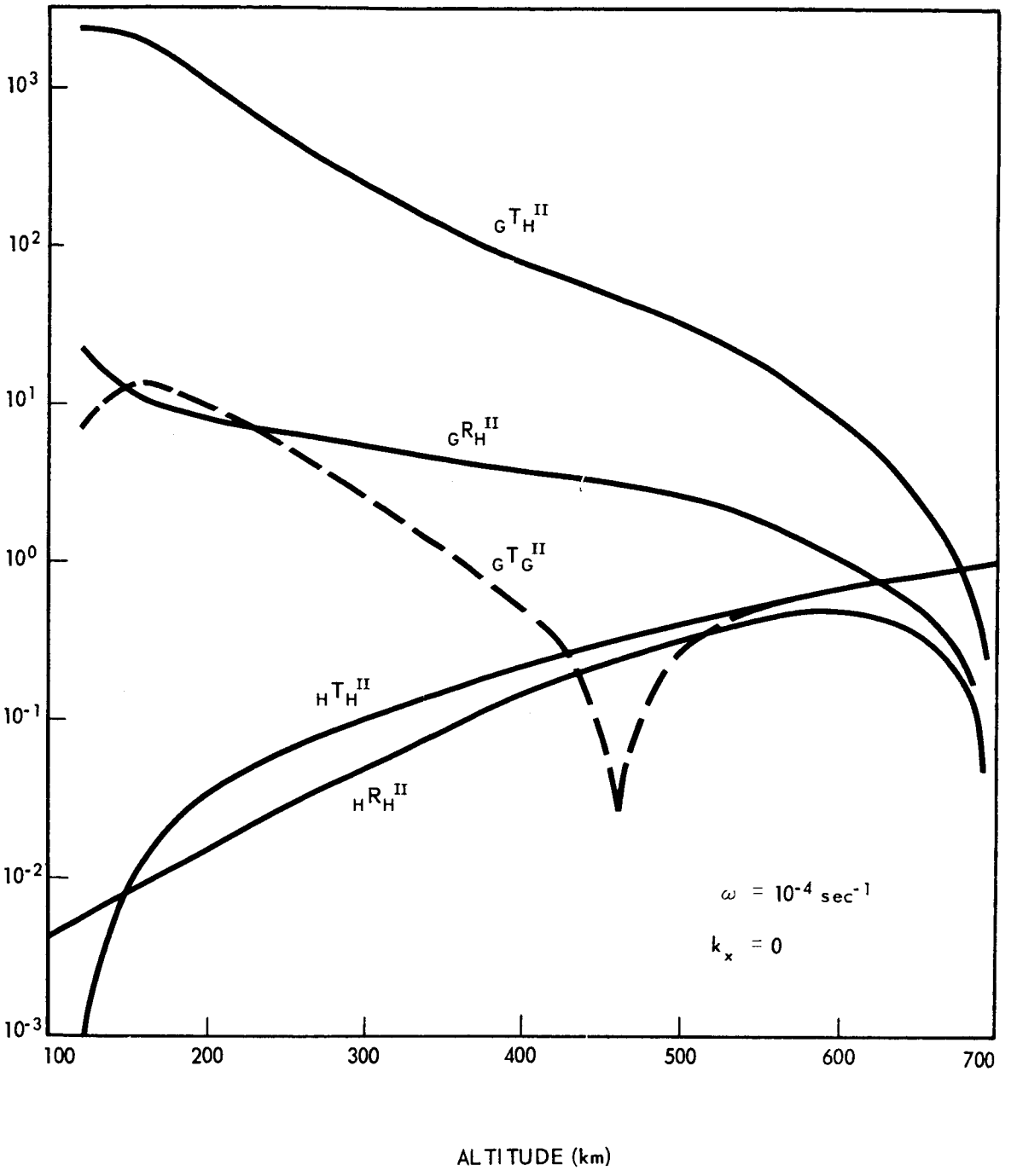

Figure 7b. Full lines: Magnitude of coefficients of reflection, transmission, conversion and coupling into gravity waves of vertically downward propagating heat conduction waves versus Z_I.

Dashed lines: Magnitude of transmission coefficients of vertically downward propagating gravity waves. Angular frequency: $\omega = 10^{-4}$ sec^{-1}.

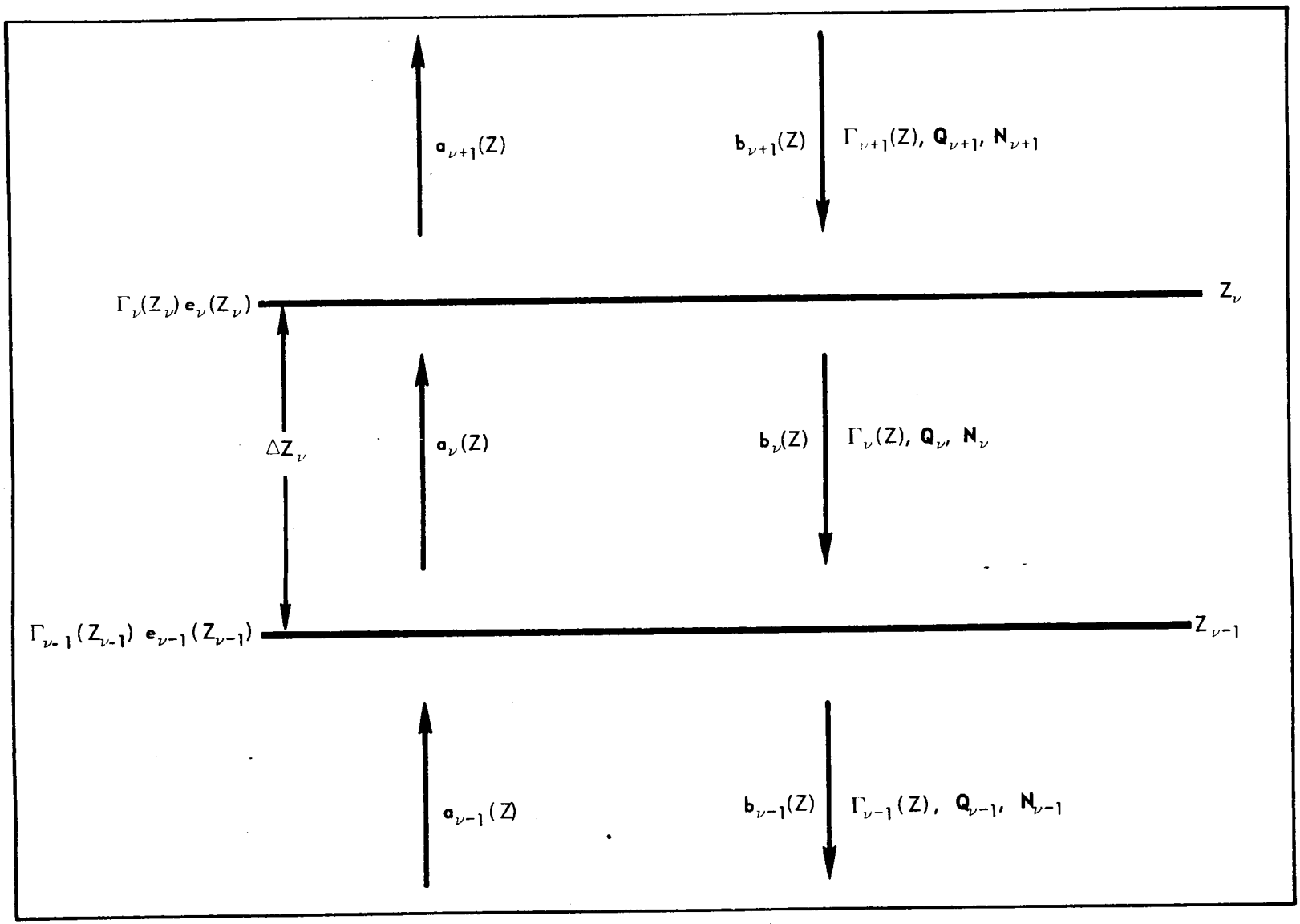

Figure D-1. The Homogeneous Slab-Model